

Flutter and long-wave instabilities in compliant channels conveying developing flows

By P. G. LAROSE¹ AND J. B. GROTBORG²

¹Mathematics and Computer Science Department, Nebraska Wesleyan University,
Lincoln, NE 68504, USA

²Departments of Biomedical Engineering and Anesthesia, Northwestern University,
Evanston, IL 60208, USA

(Received 12 July 1995 and in revised form 30 July 1996)

A partially collapsed lung airway or other flexible tube is modelled as a two-dimensional channel of infinite length. We consider the linear stability of this system conveying a developing flow, analysing the full Orr–Sommerfeld system analytically for long waves and numerically for arbitrary wavelengths. We find a long-wave instability which has not been observed in previous channel studies. This long-wave instability is stabilized by increasing the elastance of the wall, but other wall properties do not affect it except in correction terms. In addition to the long-wave instability, there is the finite wavelength (flutter) instability, which, depending on the parameter values chosen, may be critical at a higher or lower flow speed than the long-wave instability. For special parameter values the long-wave and flutter instabilities are critical at the same flow speed. Comparisons with experiments show that theoretical predictions are in agreement with experimental observations.

1. Introduction

In this study we examine the stability of developing flow through a flexible, two-dimensional channel. This is a model for systems in engineering and physiology in which flows are conveyed by compliant tubes. In many applications the tubes are short and flow speeds are large, so that consideration of a developing velocity profile is appropriate. We are specifically interested in flow through the lung airways, which can oscillate owing to wall–fluid instabilities that are thought to be the cause of wheezing lung sounds (Grotberg & Davis 1980).

There are a number of interrelated steady and unsteady behaviours that occur in flexible fluid-conveying tubes which are absent in rigid systems. If the pressure difference between the exterior and interior of such a tube is sufficiently large it may collapse. This results in a partial or complete obstruction of the tube cross-sectional area as the initially circular cross-section deforms into an oval or dumbbell shape whose aspect ratio may exceed 10. For very flexible tubes the required pressure difference may be small enough that easily attained changes in the tube environment, or the pressure drop resulting from a flow in the tube interior, may precipitate collapse. With the occurrence of collapse, the flow rate through the tube may become independent of the conditions at its downstream end (flow limited), and concurrent with or following collapse, large- or small-amplitude wall oscillations may also be seen (Shapiro 1977; Conrad 1969; Katz, Chen & Moreno 1969; Gavriely *et al.* 1989). Small-amplitude wall oscillations may also occur in more rigid (uncollapsed) tubes transporting fluids at sufficiently high velocities (Païdoussis & Issid 1974).

The oscillatory wall–fluid instabilities that are present in flexible tubes may be divided into two categories: those that require wall inertia (which we call flutter) and those that do not. Flows through flexible tubes for which the wall inertia is small by comparison with fluid inertia show various oscillatory behaviours which depend on this ratio of inertias, and which are strongly influenced by the downstream conditions in the experimental device (Bertram & Pedley 1982). The work on oscillatory instabilities dominated by fluid inertia (as is the case in the blood vessels) is the subject of a review by Kamm & Pedley (1989); we refer the reader to this for a treatment of and reference list on this subject. Flutter instabilities are higher-frequency oscillations arising from the coupling of the fluid-dynamic pressure with the compliant wall. Instabilities similar in mechanism to Kelvin–Helmholtz and water waves are among these. For the appearance of a flutter instability, a well-defined critical fluid velocity must be attained. Flow limitation is not a prerequisite for the instability, but flutter may be facilitated through the decrease in tube cross-sectional area and resulting increase in fluid flow speed that accompany limitation. In experimental studies of flutter in thick-walled tubes (Gavriely *et al.* 1989) and wheezing in the lung (Gavriely, Kelly & Grotberg 1987) these oscillatory phenomena have in fact been observed only in the presence of flow limitation.

2. Previous theoretical work

While we are specifically interested in compliant channel (or tube) flows, there is some overlap between the behaviour of such systems and that of flows over single compliant plates. The pioneering work on the interaction of flows with compliant structures is that of Benjamin and Landahl, who in the early 1960s considered the stability of boundary-layer flow over a compliant surface. Their work (Benjamin 1960, 1963; Landahl 1962) showed that the presence of a compliant boundary may significantly influence the Tollmien–Schlichting instability (TSI) and that there are also wall–fluid (flutter) instabilities which arise as a direct result of wall compliance. The latter instabilities may exist in the absence of viscosity, and each is affected differently by damping in the wall or fluid. To postpone significantly the onset of instability, it is therefore necessary to choose carefully the compliant surface so as to stabilize the TSI while avoiding the appearance of the different wall–fluid instabilities (Landahl 1962). The TSI is stabilized by the presence of the compliant surface, an effect also seen by Hains & Price (1962) for Poiseuille flow through a flexible channel. A review of this early work appears in Benjamin (1964). Carpenter & Garrad (1985, 1986) presented an in-depth analysis of the linear stability of Blasius flow over a compliant plate, in which they considered both the flutter instabilities and TSI. Flutter was investigated both analytically and numerically, and TSI numerically. Their 1985 paper also includes a review of the extensive literature on the theoretical and experimental stability analyses for flow over a flat plate, and we refer the interested reader to this and the reviews of Gad-el-Hak (1986) and Riley, Gad-el-Hak & Metcalfe (1988) for a complete overview of the subject. More recently, a multi-deck asymptotic theory for the flutter instability in this geometry was developed by Carpenter & Gajjar (1990).

Weaver & Païdoussis (1977) observed that the flutter instability seen in flattened (or collapsed) soft tubes is not the classical shell flutter mode in which the tube flattens alternately in the two perpendicular directions normal to the tube axis, but rather a ‘flapping flutter’. This flapping flutter involves the oscillation of the longer opposing walls of the flattened oval cross-section of the tube either in or out of phase with one another, and its nature suggests that it might be appropriate to model the tube as a

channel. Weaver & Païdoussis (1977) and Matsuzaki & Fung (1977) considered inviscid flow through a channel with various wall models, and found through linear analysis a divergence instability for both the symmetric and antisymmetric flutter modes when damped or finite-length models were considered. It should be noted that Weaver & Païdoussis used the method of images to find the fluid velocity. However, while this should result in an expression involving an infinite sum, they included only the first two terms, so that their solution allows cross-flow at the walls of the channel. Grotberg & Davis (1980) considered the physiological application of the flexible-channel-flow problem as a model of a collapsed airway, theorizing that wheezing lung sounds may be symptomatic of a flutter oscillation in the airway walls. They found that stability is lost to a flutter instability unless damping is also included in the wall, in which case the instability appears for lower flow speeds and is divergent. By taking the appropriate limit, Grotberg & Davis showed also that results obtained in the two-dimensional geometry are consistent with one-dimensional studies (e.g. Shapiro 1977). The drop in critical flow speed with the addition of damping was first explained by Landahl's (1962) study of flow over a compliant plate, which showed that in the absence of wall damping the system is neutrally stable prior to the instability. The addition of damping is destabilizing, and thus reduces the critical flow speed. The same effect may be obtained through the introduction of a finite axial length to the system (Lucey & Carpenter 1992, 1993). A similar drop in critical flow speed may be obtained by including fluid viscosity in the absence of wall damping, which results in the appearance of another flutter instability. This observation was made for flow over a compliant plate by Carpenter (1984), and a similar observation for flow in a compliant channel may be seen with the Grotberg & Reiss (1984) model.

In all of these channel analyses, the inclusion of damping in an infinite-length channel wall results in a divergence instability rather than an oscillatory (flutter) instability. However, in physical systems flutter is observed. To address this discrepancy, Grotberg & Reiss (1982, 1984) added a linear (hydraulic) friction term to the potential flow through a channel to approximate the effect of viscosity. It was shown by Grotberg & Shee (1985) that this approximation is consistent with results from the full Orr–Sommerfeld equation when viscosity and wall damping are taken to zero and their ratio is $O(1)$. They found that the addition of fluid friction results in the reappearance of the flutter instability, and through a weakly nonlinear analysis showed also that the bifurcation to flutter is supercritical and hence stable. Both linear and nonlinear results from this model were found to agree with collapsible tube experiments (Grotberg & Gavriely 1989).

Païdoussis & Mateescu (1987) considered the stability problem of a cylindrical shell with clamped ends conveying a developing flow, and found that the addition of viscous effects to the inviscid analysis was stabilizing. In this case, with a finite-length compliant section, no flutter was found, which is consistent with the results of Garrad & Carpenter (1982) for non-turbulent flow over a finite-length compliant plate.

The effect of a finite-depth elastic boundary on the TSI in plane Poiseuille flow was considered by Pierucci & Morales (1990), though their stability results may be influenced by their assumption that the critical wavenumber remains unchanged by the introduction of the elastic wall. There have also been a few nonlinear studies of the TSI for Poiseuille flow in a compliant channel. Rotenberry & Saffman (1990) did a weakly nonlinear analysis of the instability and derived a Ginzburg–Landau equation for the amplitude of the bifurcating solution. The channel walls they considered were simple compliant boundaries with allowance for wall damping, and they found that when these are sufficiently flexible the bifurcation to the TSI goes from being subcritical, as

is the case for a channel with rigid walls, to supercritical. Rotenberg (1992) considered the same channel system with the addition of tension to the channel walls, and inferred the criticality of the bifurcation from the shape of the curve of disturbance energy as a function of Reynolds number. He concluded that while sufficiently flexible walls may render the bifurcation supercritical, the magnitude of the supercritical branch is, in fact, very small, so that for finite but small disturbances the bifurcation appears subcritical. Thus, wall flexibility does not qualitatively change the character of the TSI in plane Poiseuille flow.

These studies show that the effects of wall and fluid damping are significant in determining the nature of the flutter instability, and also that their accurate inclusion is important in determining the nature of the observed instability. In many applications, including the lung airways, the length of the flexible tube is shorter than the entrance length of the flow. Previous studies of the flutter instability have not considered a developing flow profile. Our primary objective in this study is therefore to explore the fluid-elastic (flutter) instability with a developing flow. We choose a planar channel model for this purpose, since it allows exploration of the developing flow profile without introduction of additional issues involving the non-planar three-dimensional geometry of a collapsed tube or lung airway. Further, the use of such a model is well-motivated by previous studies, which have with success applied such models to the biofluid mechanics of lung airways and blood vessels. In the present study, we therefore consider the full linear stability problem for a developing profile in a compliant channel. In the following sections, we develop our model (§3) and present analytical (long wave) and numerical solutions (§§4–6). Because this study is motivated by an interest in flutter in the lung airways, we then make some comparisons of our theoretical results with representative previous experiments (§7) and conclude with a discussion of our results (§§8 and 9).

3. Model development

3.1. Wall and fluid equations

To model a partially collapsed flexible tube we consider a two-dimensional channel with compliant walls. Through this flows an incompressible Newtonian fluid. This is shown in figure 1. We develop the equations modelling this system in the following. The wall model is the same as, or similar to, that used in many other studies (e.g. Grotberg & Reiss 1984; Grotberg & Gavriely 1989; Carpenter & Garrad 1985, 1986), and we therefore do not present as much detail in its development as in that for the fluid flow. We consider the linear stability of the flow through the channel when the channel walls are initially flat, and therefore write the streamfunction for the fluid flow as a base state plus a disturbance, which is introduced in the usual manner using normal modes. This stream function is

$$\Psi = \Psi_0 + \psi' = \Psi_0 + \phi(z) \exp(ik(x - ct)), \quad (3.1)$$

where Ψ_0 is the stream function of the base flow, discussed below in §3.2. Here and following, lengths and velocities have been non-dimensionalized on the half-channel width b^* and an elastic wave speed of the wall, $\hat{u} = (E^*b^*/\rho^*)^{1/2}$, where E^* is the elastance (spring-constant) of the wall and ρ^* the density of the fluid. Similarly, we non-dimensionalize time on b^*/\hat{u} and pressure on $\rho^*\hat{u}^2$. Writing the (x, z) -position of a point on the wall as (U, W) , we also expand the wall position as a base state plus a disturbance,

$$(U, W) = (0, -1) + (U', W') = (0, -1) + (\chi, \zeta) \exp(ik(x - ct)). \quad (3.2)$$

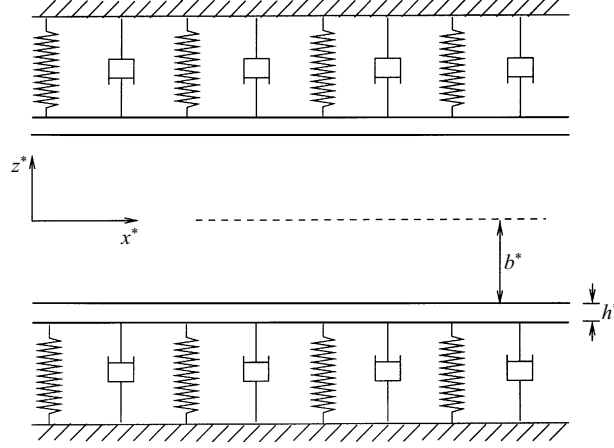


FIGURE 1. Flexible walled channel model.

The motion of the wall is given by the von Kármán plate equations (Sapir & Reiss 1979) which, after insertion of (3.2) and linearization in disturbance quantities, are:

$$(-(kc)^2 M - 2ikcG + Bk^4 + Tk^2 + 1)\zeta + \Delta S^N = 0, \quad (3.3)$$

$$(-(kc)^2 M - 2ikcH + dk^2)\chi + \Delta S^T = 0, \quad (3.4)$$

both at $z = \pm 1$. The non-dimensional parameters in (3.3) and (3.4) are: the ratio of wall to fluid mass, $M = (\rho_w^* h^* / \rho^* b^*)$; normal and tangential wall damping $G = Mb^* G^* / \hat{u}$ and $H = Mb^* H^* / \hat{u}$; bending stiffness $d = 12 D^* / h^{*2} b^* \rho^* \hat{u}^2$; flexural rigidity $B = D^* / b^{*3} \rho^* \hat{u}^2$; imposed longitudinal tension $T = T^* / b^* \rho^* \hat{u}^2$; and, normal and tangential fluid stresses ΔS^N and ΔS^T . The elastance (spring-constant) is $E = E^* b^* / \rho^* \hat{u}^2$, which equals one for our choice of scales. Dimensional parameters appearing in these are the wall density ρ_w^* , wall thickness h^* , normal and tangential wall damping G^* and H^* , flexural rigidity D^* , and imposed tension T^* . Assuming deflections of the plate to be small, the stresses in (3.3) and (3.4) are

$$\Delta S^N = -\Delta p + \frac{-2\psi'_{xz}}{R_w}, \quad \Delta S^T = \frac{\psi'_{zz} - \psi'_{xx}}{R_w}, \quad (3.5)$$

where $R_w = \hat{u} b^* / \nu$ is the Reynolds number and Δp the difference between the fluid and external pressures. We have chosen the notation R_w to emphasize that this Reynolds number, owing to our choice of velocity scale as a wall elastic wave speed, is related to the wall elastance.

The fluid flow must satisfy the Navier–Stokes equations, which, after linearization, give the Orr–Sommerfeld equation,

$$k(u_0 - c)(\phi'' - k^2 \phi) - k u_0' \phi + \frac{i}{R_w}(\phi^{iv} - 2k^2 \phi'' + k^4 \phi) = 0, \quad (3.6)$$

assuming that the base flow given by Ψ_0 is parallel so that $u_0(z) = d\Psi_0/dz$ is the base axial flow velocity in the channel. At the channel wall, the fluid must satisfy the linearized kinematic and no-slip conditions,

$$kc^2 \chi = i(\phi' c + \phi u_0'), \quad \phi = c\omega, \quad (3.7)$$

where u_0 and ϕ are, after linearization, evaluated at $z = \pm 1$.

With (3.5), (3.1) and (3.7), the wall equations (3.3) and (3.4) become (after elimination of the pressure from (3.5) using the Navier–Stokes equations)

$$(-(kc)^2M - 2ikcG + Bk^4 + Tk^2 + 1)k\phi + kc^2\phi' + kcu'_0\phi - \frac{ic}{R_w}(\phi''' - 3k^2\phi') = 0, \quad (3.8)$$

$$(-(kc)^2M - 2ikcH + dk^2)(c\phi' + \phi u'_0) + \frac{ikc^2}{R_w}(\phi'' + k^2\phi) = 0, \quad (3.9)$$

both at $z = \pm 1$.

Solution of the linear stability problem then requires us to find a solution to the Orr–Sommerfeld equation (3.6) with boundary conditions (3.8) and (3.9). By assuming disturbances to be separated into ‘symmetric’ and ‘antisymmetric’ modes we may restrict attention to the lower half of the channel. For symmetric disturbances the channel walls oscillate out of phase with one another (in a varicose shape) so that the disturbance streamfunction must satisfy conditions of no cross-flow at the midline; for antisymmetric disturbances the walls are in phase (a sinuous shape) and we require no axial flow at the midline. These conditions are

$$\text{or} \quad \left. \begin{aligned} \phi(0) = \phi''(0) = 0 & \quad (\text{symmetric}), \\ \phi'(0) = \phi'''(0) = 0 & \quad (\text{antisymmetric}). \end{aligned} \right\} \quad (3.10)$$

For simplicity, we assume that tangential wall inertia and damping may be neglected, that is, that we may discard the first two terms in the tangential boundary condition (3.9); comparison of numerical results for the resulting modified boundary condition with those with the full condition shows the two to be indistinguishable. If the tangential stress is also omitted from (3.9) we recover the no-slip condition used by Benjamin (1960) and others, which does not include horizontal wall motion.

3.2. Specification of the base flow profile

To complete the specification of the Orr–Sommerfeld system derived in §3.1, a base flow profile must be chosen. As a solution for flow in a channel, this will be either a developing (boundary layer) or developed (plane-Poiseuille) flow. We are interested in modelling short tubes, and so are concerned with the developing flow profile. There is no closed-form solution for the developing flow stream function, and we therefore follow Schlichting (1934; see also 1955) to obtain a perturbation solution,

$$u_0 = S(f'_1(\eta) + \epsilon f'_2(\eta) + \epsilon^2 f'_3(\eta) + \dots), \quad (3.11)$$

where $\epsilon \equiv (\nu^*x^*/b^*S^*)^{1/2}$ (S^* = the velocity of the initial (uniform) flow (thus, S^*b^* is the flow rate through the channel); $S = S^*/\hat{u}$), f_1 is the Blasius stream function, and η is the Blasius similarity variable $(z^* + b^*)/(\nu^*x^*/S^*)^{1/2}$. In non-dimensional variables, $\epsilon = (x/SR_w)^{1/2}$ and $\eta = (z+1)/\epsilon(x)$. Solution for the correction terms, f_2 and f_3 , is straightforward, so that we do not elaborate here (for details see LaRose 1994).

In the derivation of the Orr–Sommerfeld equation, u_0 was assumed to be a function of z only; we thus evaluate ϵ for a fixed value of $x = x_0$ to eliminate the dependence of u_0 on the axial coordinate. Because ϵ changes as $x^{1/2}$ it is necessary to impose a downstream limit on x_0 to maintain the validity of the perturbation solution for u_0 . Following Schlichting (1934; 1955) we choose to restrict x_0 so that ϵ is sufficiently small and the successive terms of the solution for u_0 remain well ordered, i.e. $f'_1 > \epsilon f'_2 > \epsilon^2 f'_3$. This requires that ϵ be less than 0.1455, or by extension that we choose $x_0 < (0.1455)^2 R_w S$. If additional terms are included in the expansion for u_0 the downstream constraint on x_0 becomes more severe (e.g. Collins & Schowalter (1962) cite $\epsilon < 0.0707$ ($x_0 < 0.005 R_w S$) for a seven-term expansion). Comparison of the

resulting velocity profile with a second-order finite-difference solution of the boundary-layer equations shows that for positions x_0 within this region of validity the perturbation solution is very good (LaRose 1994). For the base profile to be assumed to be independent of x , we must also select x_0 to be large enough for the flow to be locally parallel. We return to this issue in §4 and in the discussion in §9.

4. Solution for long waves

While it is in general difficult to solve the Orr–Sommerfeld system analytically, a solution for the case of long waves ($k \rightarrow 0$) is more tractable. Note that the following analysis is general to arbitrary flow profiles; we consider specific cases after the derivation. For $k \ll 1$, let

$$\phi \sim \phi_0 + k\phi_1 + \dots, \quad c \sim c_0 + kc_1 + \dots \quad (4.1)$$

Using these in the Orr–Sommerfeld equation (3.7) and letting $k \rightarrow 0$, we obtain

$$\phi_0^{\text{iv}} = 0, \quad (4.2)$$

so that ϕ_0 is a cubic polynomial in z . Imposing the boundary conditions (3.10) and the leading-order forms of (3.8) and (3.9) (and assuming for (3.9) no horizontal wall motion to simplify the analysis), we find

$$\phi_0 = z, \quad c_0 = u'_0(z = -1). \quad (4.3)$$

Here we have normalized ϕ_0 so that $|\phi_0(-1)| = 1$. The solution (4.3) is for symmetric disturbances only; we address the antisymmetric mode below. We see from (4.3) that c_0 is strictly real, and so must continue to the next order in k to evaluate the stability of the system.

At order k , the Orr–Sommerfeld equation (3.6) is

$$\phi_1^{\text{iv}} = -iR_w z u_0'' \quad (4.4)$$

and ϕ_1 is thus the sum of another cubic polynomial in z and a particular solution. After integration by parts once, the particular solution satisfies

$$\phi_{1P}''' = iR_w(u_0 - z u_0'). \quad (4.5)$$

Further integration is dependent on the choice of the base flow u_0 . Applying the boundary conditions (3.10) and the order k terms of (3.8), we find

$$\phi_1 = -\phi_{1P}(z=0) + B_1 z - \frac{1}{2}(\phi_{1P}''(z=0))z^2 + \frac{iR_w[1 - (u_0'(z=-1))^2]}{6u_0'(z=-1)}z^3 + \phi_{1P}, \quad (4.6)$$

so that, from (3.9),

$$c_1 = iR_w \left[u_0'(z=-1) [\Phi_{1P}(z=0) - \frac{1}{2}\Phi_{1P}''(z=0) - \Phi_{1P}(z=-1) - \Phi_{1P}'(z=-1)] - \frac{1}{3u_0'(z=-1)} [1 - (u_0'(z=-1))^2] \right], \quad (4.7)$$

where we have written $\phi_{1P} = iR_w \Phi_{1P}$ to make the imaginary character of c_1 explicit.

Equation (4.7) for c_1 is strictly imaginary, so that c_1 is the growth rate for the disturbance. To find the critical flow speed at which c_1 becomes positive, it is necessary

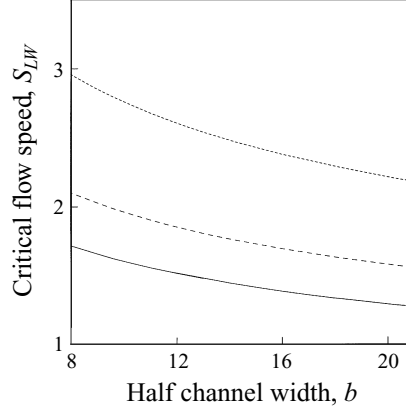


FIGURE 2. Critical flow speeds for long-wave instability as functions of half-channel width and elastance. b^* scaled on x_0^* , S^* on $10^{-2} (\nu^*/x_0^*)$. —, $R_w = 2230$; ---, $R_w = 3000$; ···, $R_w = 5000$ (where $R_w \equiv (\dot{u}x_0^*/\nu)$ and $\dot{u} = (E^*x_0^*/\rho^*)^{1/2}$). ($x_0 = 1$.)

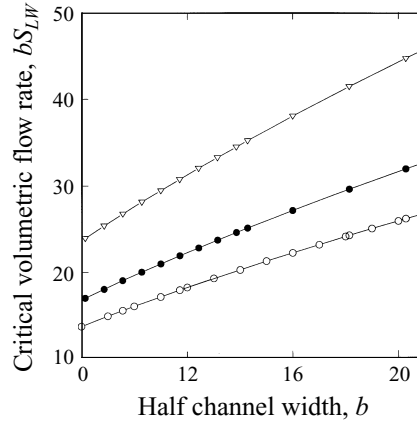


FIGURE 3. Critical volumetric flow rate for long-wave instability as a function of half-channel width and elastance. Scales and parameter values as in figure 2. \circ , $R_w = 2230$; \bullet , $R_w = 3000$; ∇ , $R_w = 5000$.

to integrate expression (4.5) for ϕ_{1P} . We consider two cases. For plane-Poiseuille flow, $u_0 = 1.5S(1-z^2)$, and we may integrate to find ϕ_{1P} and evaluate (4.7) analytically, obtaining $c_1 = 0.067iR_w(18S^2 - 5)$. Instability appears at a flow speed $S_{LW} = 0.527$; at this point $c_0 = u_0'(-1) = 1.581$. These are in good agreement with the numerical solution (described in §5), which gives $S_{LW} = 0.525$ and $c_0 = 1.575$ at $k = 0.001$. For channel flow, we numerically integrate (4.5) using Simpson's rule, and find (for $R_w = 2230$ and $x = 1$) $S_{LW} = 0.1387$ and $c_0 = 1.094$. These agree with the numerical values for the critical flow speed to within 10% for $k \leq 0.014$, and at $k = 0.001$ we find numerically that $S_{LW} = 0.1388$ and $c = 1.093$. The existence of the long-wave instability is also useful for the numerical solution, as it gives starting points from which the stability calculation may proceed.

The effect of varying the half-channel width and wall elastance on the long-wave stability boundary for developing flow is shown in figures 2 and 3, in which the long-wave critical flow speed S_{LW} and volumetric flow rate, bS_{LW} are plotted as functions of the half-channel width and wall elastance. In both figures, flow speeds and half-

channel width are scaled on (ν/x_0^*) and x_0^* , respectively, to isolate the effect of changing b . Curves for different values of the wall elastance are shown in both figures. These figures show that the critical flow speed increases as channel width is decreased, but that the critical volumetric flow rate decreases. Increasing the wall elastic modulus increases both the critical flow speed and flow rate. Note that the long-wave stability bounds do not depend on the wall properties other than the elastance; the effects of the mass ratio M , bending stiffness B , etc. appear only at higher orders in k .

The above treatment was strictly for the case of symmetric disturbances. When antisymmetric disturbances are considered the analysis proceeds in much the same manner, with the midline boundary conditions replaced by the antisymmetric forms of (3.10). In this case the leading-order term of the wall condition (3.8) and the second midline condition are redundant, so that the solution for the leading-order antisymmetric eigenfunction and eigenvalue ϕ_{A_0} and c_{A_0} becomes a one-parameter family of solutions,

$$\phi_{A_0} = A_{A_0} + D_{A_0} z^2, \quad c_{A_0} = \frac{A_{A_0} + D_{A_0}}{2D_{A_0}} u'_0(z = -1), \quad (4.8)$$

(for normalization we may specify one of A_{A_0} or D_{A_0} ; when possible we take $A_{A_0} = 1$) provided the free parameter D_{A_0} is non-zero. If D_{A_0} is zero the second wall condition, (3.9), requires $A_{A_0} = 0$, and the solution for ϕ_{A_0} is trivial. At $O(k)$, condition (3.8) becomes a condition on D_{A_0} , and requires it to be zero. Thus the only eigenfunction is the trivial one, and there is no long-wave antisymmetric instability.

It may be noted at this juncture that in the limit of long waves the assumption of locally parallel developing flow made in the derivation of the Orr–Sommerfeld equation is violated. Thus, in this limit, the developing flow result would be somewhat different if non-parallel effects were included. However, while studies such as Hall & Smith (1984) and Fasel & Konzelmann (1990) demonstrate the influence of non-parallelism on Tollmein–Schlichting instabilities, the body of this work has only considered flow with rigid boundaries. We consider these works and others in greater detail in §9. As flutter instabilities are generally dominated by wall (rather than fluid) effects, it is not clear how these results would apply to flutter, and there may be some hope that the fundamental nature of the long-wave instability would not be altered by non-parallelism in the flow. We speculate that the long-wave instability may be related to further collapse of the flexible tube but clearly (owing both to our choice of geometry and the issue of non-parallelism) are unable at this juncture to investigate this. Note that if the wall boundary conditions (3.8) and (3.9) are replaced by those for a rigid wall, $\phi(z = -1) = \phi'(z = -1) = 0$, the solution for either symmetric or antisymmetric disturbances is trivial, confirming that the long-wave instability is a function of wall flexibility.

5. Numerical solution method

To solve the Orr–Sommerfeld system (3.6) and (3.8)–(3.10) numerically we use a multiple shooting method with orthonormalization (Davey 1973), with modifications to accommodate the presence of the compliant wall (LaRose 1994). Briefly, we define the orthonormalized transfer matrix \mathbf{C} as in Davey's paper to be that matrix which, when multiplied against an initial condition $\phi_0 (= (\phi, \phi', \phi'', \phi''')^T)$ for ϕ at the channel midline, gives an integration of ϕ_0 at the wall which preserves the singularity necessary for the determination of the eigenvalue c through application of the boundary

Case	Present work		Previous result	
	Re_{CR}	k_{CR}	Re_{CR}	k_{CR}
Plane Poiseuille flow	5772.2	1.021	5772.2	1.021 [HDR]
Developing channel flow, $x = 100$	9383	1.67	9790 [GG]	
	$x = 170$	8330	1.34	8420 [GG]
Single plate (Blasius) flow	519.7	0.305	520	0.301 [J]

TABLE 1. Comparison of critical Reynolds and wavenumbers for TSI in flows with rigid boundaries. [HDR] Hughes, in Drazin & Reid (1981), [GG] Gupta & Garg (1981) (from their figure 1), [J] Jordinson (1970). (Values of k_{CR} for the results of Gupta & Garg are difficult to obtain accurately from their figures and so are omitted.)

conditions there. With the boundary conditions at the wall defined by the vector operators \mathbf{B}_1 and \mathbf{B}_2 (so that the i th element of \mathbf{B}_j is the coefficient of the $(i-1)$ th derivatives of ϕ found in equations (3.8) or (3.9)), the boundary conditions at the wall may be written as

$$\begin{pmatrix} \mathbf{B}_1^T \\ \mathbf{B}_2^T \end{pmatrix} \mathbf{C} \phi_0 = \begin{pmatrix} 0 \\ 0 \end{pmatrix}. \quad (5.1)$$

For the channel problem, the initial condition ϕ_0 is chosen to satisfy either the symmetric boundary conditions $\phi(0) = \phi''(0) = 0$ or the antisymmetric boundary conditions $\phi'(0) = \phi'''(0) = 0$, so that ϕ_0 will be a linear combination of two basis vectors: either $\phi_0 = (0, a_1, 0, a_2)$ or $\phi_0 = (a_1, 0, a_2, 0)$. Thus for condition (5.1) to have a non-trivial solution the eigenvalue c must be found to satisfy the determinant condition

$$(\mathbf{B}_1 \cdot \mathbf{c}_2)(\mathbf{B}_2 \cdot \mathbf{c}_4) - (\mathbf{B}_1 \cdot \mathbf{c}_4)(\mathbf{B}_2 \cdot \mathbf{c}_2) = 0, \quad (5.2)$$

(for symmetric disturbances) where \mathbf{c}_j indicates the j th column of the transfer matrix \mathbf{C} .

In some cases (e.g. if the flow over a single compliant surface is of interest) the boundary conditions at the ‘channel midline’ (which for flow over a single surface is equivalent to ‘infinity’) cannot be written as a linear combination of two basis vectors, as was the case above. In this case, to preserve the outlined method, we introduce a new variable $\hat{\phi} = \mathbf{H}\phi$, where the matrix \mathbf{H} is chosen to transform the boundary conditions at the ‘channel midline’ to a simple form such as $\hat{\phi}(0) = \hat{\phi}''(0) = 0$. The modified system is then solved for $\hat{\phi}$ as indicated above, bearing in mind that the integration routine and boundary conditions \mathbf{B}_j must be modified to take into account the transformation of ϕ by \mathbf{H} .

To verify the accuracy of this method, we next compare results from our stability calculations with a number of known stability results for different geometries and boundary conditions.

5.1. Comparison for flows with rigid boundaries

In geometries bounded by rigid plates we scale velocity on the flow speed of the base flow profile, and lengths on the half-channel width (for channels) or the displacement thickness of the boundary layer (for flow over a single plate). In table 1 we show the stability results we obtain for the TSI for plane-Poiseuille and developing channel flow, and for Blasius flow over a single plate. These are compared with previous results. The agreement is seen in all cases to be very good. The lack of exact agreement with the

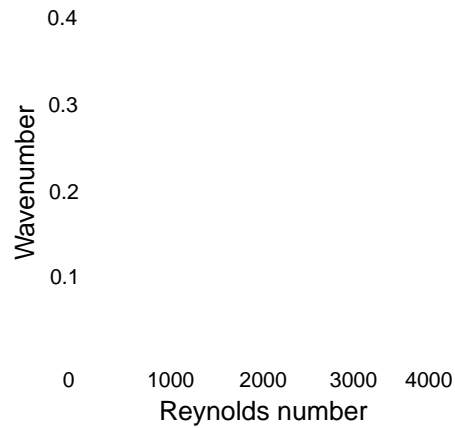


Figure 4. Neutral stability curve for Blasius flow over a compliant plate, TSI; comparison between α , results of Carpenter & Garrad (1985) and α , present work. Elasticity 0.3 N mm^{-2} .

Reynolds number	Present work, range of unstable wavenumbers	Range of unstable wavenumbers [CG]
4000	0.050 ± 0.130 0.142 ± 0.344	0.051 ± 0.131 0.146 ± 0.343
4500	0.070 ± 0.142 0.158 ± 0.380	0.069 ± 0.145 0.159 ± 0.380

Table 2. Comparison of Blasius flutter roots from present and past work, scaled on maximum flow speed and boundary-layer displacement thickness. [CG] results of Carpenter & Garrad (1986, from their figure 13). $E = 0.5 \text{ N mm}^{-2}$.

developing channel flow results of Gupta & Garg (1981) we attribute to differences in

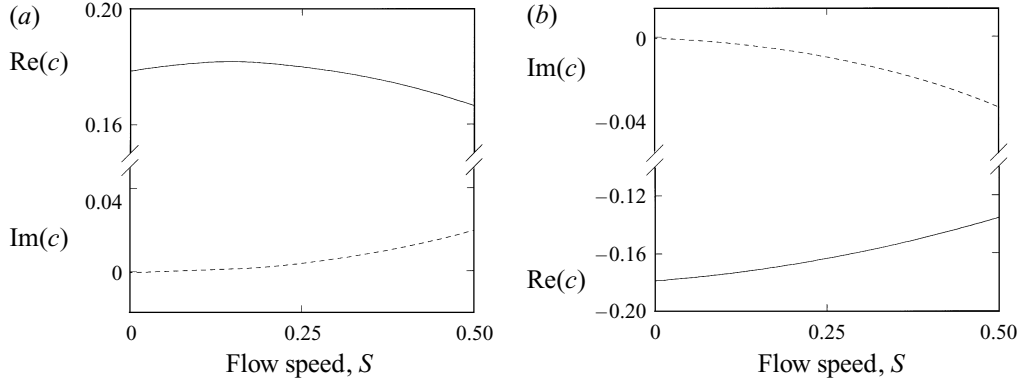


FIGURE 5. Developing flow flutter dispersion relation as a function of flow speed. (a) root 1; (b) root 2. ---, $\text{imag}(c)$, —, $\text{real}(c)$ ($M = 2190$, $B = 540$, $T = 0$, $G = 0.054$, $d = 882$, $R_w = 2230$, $k = 0.1$, $x_0 = 1.0$).

6. Results

For the results presented below, we use parameter values to model a collapsed thick-walled tube, as given in Gavriely *et al.* (1989). The dimensionless values are given in the figure caption for figure 5, and correspond to the dimensional values $\rho_w^* = 0.941 \text{ g cm}^{-3}$, $h^* = 0.9 \text{ cm}$, $\rho^* = 8 \times 10^{-4} \text{ g cm}^{-3}$, $b^* = 0.07 \text{ cm}$, $\nu^* = 0.225 \text{ cm}^2 \text{ s}^{-1}$, $G^* = 1.72 \text{ s}^{-1}$, $T^* = 0$, $E^* = 5.86 \times 10^5 \text{ dyne cm}^{-3}$, and $D^* = 7621 \text{ dyne cm}$.

The flutter dispersion relation has two roots, shown in figure 5(a) as functions of the flow speed S . At zero flow speed these have equal decay rates and phase speeds of equal magnitude but opposite sign. We designate the initially downstream travelling wave (positive $\text{real}(c)$) as root 1 and the other as root 2. Root 1 is that which becomes unstable first as S is increased, and is a Type B wave as defined by Benjamin (1963) and Landahl (1962). Root 2, which is initially upstream travelling, slows as the flow speed is increased until for some flow speed S_D it reverses direction to become downstream travelling. In simpler systems (Grotberg & Davis 1980), reversal of this wave was interpreted as signifying flow limitation or ‘choked flow’ (Shapiro 1977). In figure 5(a) (and 5b) we see a flutter instability at a lower flow speed than S_D , which is consistent with our use of parameter values to model an already collapsed flexible tube, for which flutter is expected. When large wall-to-fluid mass ratios are considered (as are appropriate for the lung airway) the flow may be insufficient to reverse the direction of root 2 for small to moderate flow speeds, so that it remains upstream travelling until significantly after the onset of instability in root 1 (as shown in figure 5b).

Neutral stability curves for the symmetric and antisymmetric flutter instabilities are shown in figure 6, giving critical flow speeds as a function of wavenumber. Points below (above) the curves are stable (unstable). The limit of $k \rightarrow 0$ on these curves gives S_{LW} , and the local minimum for $k > 0$ gives the critical flow speed for the oscillatory (flutter) instability, S_F . We denote the minimum of S_{LW} and S_F as S_{CR} , the flow speed at which instability is first seen. In figure 6 the symmetric mode is seen to be the least stable, and as $S_F < S_{LW}$ flutter is seen rather than the long-wave instability. However, by varying another parameter, for example the mass ratio M , we can shift the critical flow speed to S_{LW} . In figure 7 neutral stability curves are shown for a number of different mass ratios. Reduction of the mass ratio M stabilizes the flutter instability, so that the instability moves from non-zero to zero wavenumber as M is decreased. Once the long-wave instability has appeared, further variation in M does not alter the onset

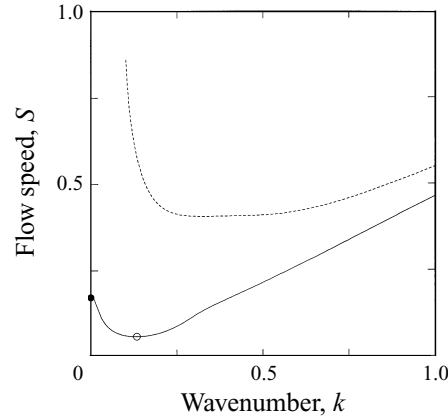


FIGURE 6. Neutral stability curves, flutter instability. —, symmetric mode; ---, antisymmetric, ●, S_{LW} ; ○, S_F ($M = 3190$, $B = 542$, $T = 0$, $G = 0.054$, $d = 882$, $R_w = 2230$, $x_0 = 2.0$).

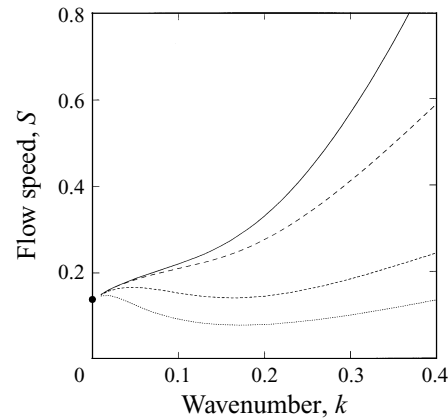


FIGURE 7. Neutral stability curves for different mass ratios, showing long-wave instability. ●, long-wave limit. ·····, $M = 500$; ---, $M = 100$; - · - ·, $M = 100$; —, $M = 1$ ($B = 542$, $T = 0$, $G = 1.69 \times 10^{-5}$, $d = 882$, $R_w = 2230$, $x_0 = 1.0$).

flow speed of the instability. This transition between the finite- and long-wavelength instabilities admits the appearance of a co-dimension two bifurcation point, occurring when the long-wave and flutter instabilities have the same critical flow speed. Note that as the mass ratio appears in the definition of the wall damping G , to isolate the effect of variation in M it is necessary to allow G to change while holding $\hat{G} (\equiv b^*G^*/\hat{u})$ fixed.

In figures 8(a) and 9(a) the effect of variation of the wall damping G and wall elastance on the stability of the system is shown, in figure 8(a) by plotting S_{LW} and S_F , and in figure 9(a) by plotting S_F (for the range of parameter values shown in figure 9, $S_F < S_{LW}$) as functions of these variables. In figure 8, curves for different values of M are plotted to show the destabilizing effect of increasing inertia, and in figure 9 the stabilizing effect of increasing the wall flexural rigidity (B) is also shown. Figures 8(b) and 9(b) show the frequency of the oscillations appearing at S_{CR} . Note the discontinuous change in the frequencies shown in figure 8(a) arising from the appearance of the long-wave instability. Because E^* appears in the definition of the velocity scale \hat{u} , in figure 9 velocities are scaled on the viscous velocity scale (ν^*/b^*) and

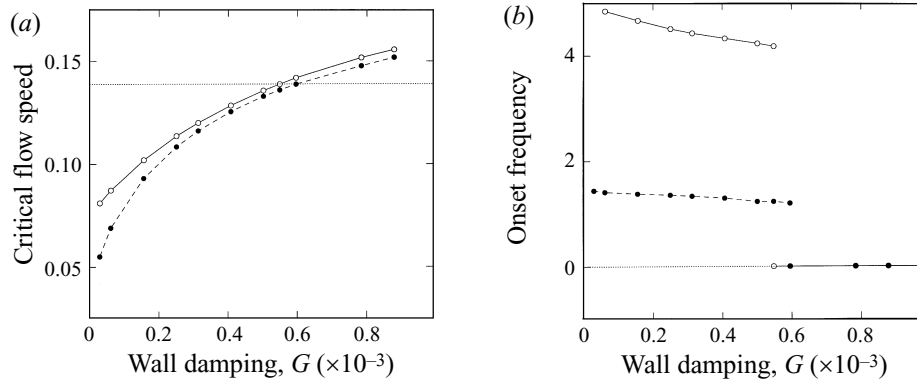


FIGURE 8. (a) Critical flow speeds S_{LW} and S_F and (b) frequency at S_{CR} as functions of wall damping and mass ratio. $\cdots\cdots$, S_{LW} ; Symbols give S_F in (a) and frequency in (b): \circ , $M = 5000$; \bullet , $M = 500$ ($B = 542$, $T = 0$, $d = 882$, $R_w = 2230$, $x_0 = 1.0$).

E^* on $(\rho^* \nu^{*2} / b^{*3}) \times 10^4$. Increasing either G or the wall elastance stabilizes the flutter instability, which may be expected, as the flutter root going unstable is a Type B wave, which is stabilized by wall damping, and increasing E (stiffening the wall) is also known to stabilize the flutter instability. In a rigid channel the flutter instability does not exist. Similarly, figure 9(a) also shows that increasing B stabilizes the system. As shown in the inset in the figure, this is most pronounced for larger values of the elastance, for which the instability has a shorter wavelength. This is as expected, and a similar effect may be obtained through variation of the wall tension T . From figure 9(b) it is seen that the critical flutter frequency goes approximately as $E^{1/2}$, which is consistent with the results of Grotberg & Reiss (1984). Note that the second wall stiffness parameter, d , is not independent of B , varying only by a factor of 12 $(b^*/h^*)^2$. We have retained it as a second parameter only to facilitate comparison with the results obtained for the limit of no horizontal wall motion (which corresponds to $d^{-1} \rightarrow 0$). We find little quantitative difference between the cases $d^{-1} = 0$ and $d^{-1} \neq 0$, which is reasonable given the value of d for the systems we consider, $d = 882$.

Because the half-channel width b^* also appears in the scaling of the problem, to examine the effect of changing b^* we scale the system as noted in §4, scaling lengths on x_0^* and velocities on (ν^*/x_0^*) . Figure 10 shows the neutral stability curves for a number of different half-channel widths b . As b is increased, the effect of the second plate and hence of viscosity in the channel is decreased, which stabilizes Type B waves. However, as indicated in §4, the long-wave instability continues to appear at lower flow speeds, so that for sufficiently wide channels instability is lost to the long-wave instability while for a narrower channel, flutter will be seen. This is also seen in figure 11, which shows S_{LW} and S_F as functions of b . We see that as b is increased past ≈ 6 –9 the instability goes from the flutter to the long wavelength instability.

This appearance of the long wave (collapse) instability for wide channels and flutter for narrower ones is consistent with physical observations. Experiments of flow through flexible tubes (Gavriely *et al.* 1989) have shown that flutter only occurs following tube collapse. Additionally, in the course of expiration the diameter of the lung airways decreases, so that it should be expected from our theoretical predictions that collapse should be seen before wheezing (flutter), as it is in Gavriely *et al.* (1987). In figure 11, curves are given for two values of the wall elastance (and hence R_w), showing that as the wall elastance is increased the codimension two point shifts to

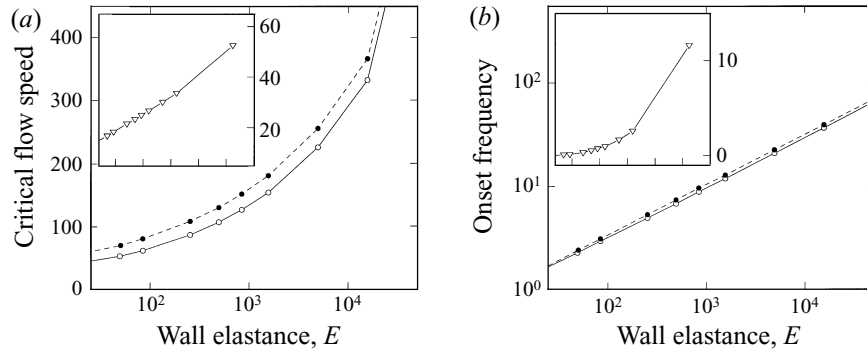


FIGURE 9. (a) Critical flow speed S_{CR} ($= S_F$) and (b) flutter frequency as functions of the wall elastance E . Elastance scaled on $(\rho^* \nu^{*2} / b^{*3}) \times 10^4$, velocity on (ν^* / b^*) , frequency on (ν^* / b^{*2}) . \bullet , $B = 2.688 \times 10^5$; \circ , $B = 2.688 \times 10^4$. Inset plots give the difference between S_{CR} and f_{CR} for the two values of b , as a function of E . (Other parameters as figure 7 ($M = 3190$), with modified scaling.)

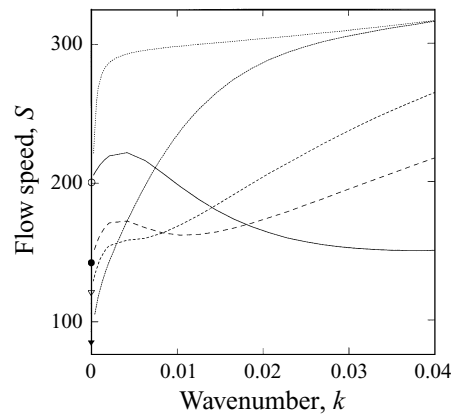


FIGURE 10. Neutral stability curves for different channel widths, showing long-wave instability and comparison with Blasius flow over a single compliant plate. Lengths scaled on x_0^* , velocities on (ν^* / x_0^*) . Symbols at $k = 0$ identify curves: \circ , $b = 4.82$; \bullet , $b = 14.5$; ∇ , $b = 24.1$; \blacktriangledown , $b = 72.4$; \cdots , Blasius flow over a single compliant plate. Other parameters as figure 7 ($M = 3190$), with modified scaling.

larger channel widths. This is consistent with the correlation between the long-wave instability and tube collapse. In stiffer tubes, the flutter instability is seen in the absence of collapse, indicating that the codimension two point has in those cases shifted sufficiently to guarantee the appearance of the flutter instability. Also, the onset of wheezing in the lung is quite sudden, consistent with decreasing airway diameter causing a shift from a long-wave to a flutter instability.

As the half-channel width is increased the perturbation solution for the developing flow that we are using converges to Blasius flow over a single compliant plate, and the stability results for the single plate system (e.g. Carpenter & Garrad 1986) are recovered for the finite wavenumber instability. However, for long waves the effect of the opposing channel wall is always significant, so that the single plate limit is not reached; this is shown in figure 10 through the inclusion of a stability curve for Blasius flow over a single compliant plate.

Also as the half-channel width is increased, some confusion appears in the resolution of the flutter root in the vicinity of the point at which the maximum speed of the flow

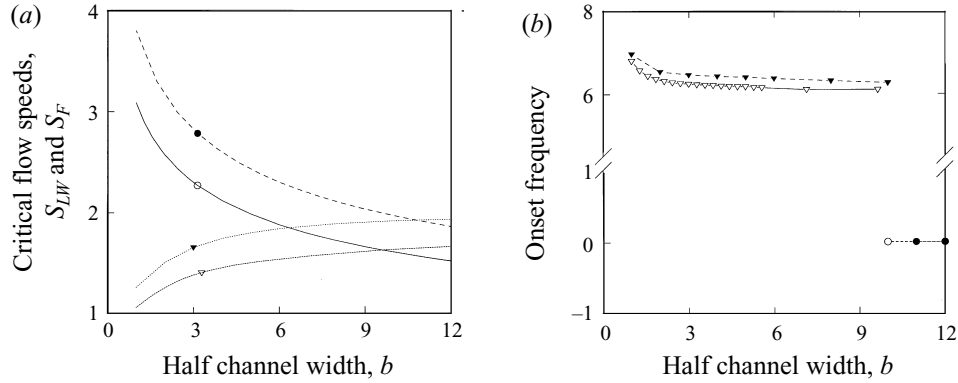


FIGURE 11. (a) Critical flow speeds S_{LW} and S_F and frequency at (b) S_{CR} as functions of the half-channel width and elastance. S_{LW} : \circ , $R_w = 2230$; \bullet , $R_w = 3000$; S_F : ∇ , $R_w = 2230$; \blacktriangledown , $R_w = 3000$ (where $\tilde{R}_w \equiv (\tilde{u}x_0^*/\nu)$ and $\tilde{u} = (E^*x_0^*/\rho^*)^{1/2}$; $x_0 = 1$, other parameters as figure 7 ($M = 3190$)). In (a), symbols serve to identify curves, not specific data points.)

and phase speed of the disturbance become equal. This is due to the existence in the infinite (single plate) system of a continuous eigenvalue spectrum along this line (Grosch & Salwan 1978; Craik 1991). While there is no continuous spectrum in the finite width (channel) system (Lin 1961), as the channel is modified to look more like the infinite case (when the channel width is increased, or other parameters altered to obtain the same effective result) the numerical solution may be expected to encounter difficulty in resolving the root as the phase speed of the disturbance becomes similar to the flow speed of the base flow.

Because increasing the Reynolds number of the flow is equivalent to decreasing the fluid viscosity, such an increase stabilizes the flutter instability. However, in the case of the developing profile, increasing the Reynolds number also changes the base flow profile, causing a narrowing of the boundary layer at the wall for constant flow speed S and axial position x_0 . A similar effect may be obtained by decreasing x_0 . This destabilizes the flutter instability. It is difficult to draw conclusions for wide ranges of axial positions, however, owing to limitations imposed by the downstream limit of validity for our developing profile. Further, as points farther upstream are considered, non-parallelism in the flow may become significant. This is discussed in §9.

Wheezing lung sounds are thought to be symptomatic of airway flutter (Grotberg & Davis 1980). Thus the characteristics that distinguish the lungs of wheezing patients from healthy subjects should relate to those effects that destabilize the flutter instability. We say above that these destabilizing effects include reduction of the wall elastance and bending stiffness, and reduction of the half-channel width, all characteristics of asthmatic and emphysematous patients' airways.

7. Specific comparison with experiments

As our motivation for beginning this study is flutter in the lung airways, we next make some comparisons between the model developed in the preceding sections and physical systems. In that the model is based on a planar channel model while the experiments with which we are comparing exhibit non-planar, three-dimensional geometries it is clear that the comparisons are in some sense preliminary – however, given that the important mechanisms of the fluid–wall interaction are present in the planar model, we hope for at least qualitative agreement between the model and the

experimental results. First, we compare with some wheezing experiments, and subsequently with experiments with flexible tubes.

The characteristics of the lung airways that we need to obtain the parameters in our model (M , B , etc.) are unfortunately not known with sufficient accuracy to allow a quantitative comparison with experiments. To obtain these parameter values, we use estimates for the lung airway characteristics used in Dragon & Grotberg (1991) and available from Olson, Dart & Filley (1970) (details may be found in LaRose 1994), and obtain wheezing (flutter) frequencies of 508–1808 Hz. These are in good agreement with the forced expiratory wheeze experiments (Gavriely *et al.* 1987), which report wheezing frequencies of 580–2730 Hz. There are two explanations for the experimental range of frequencies being higher than the theoretical predictions: one is inaccuracy in the parameter estimates used to obtain the theoretical results, and the other that we cannot be sure that the experimental frequencies are those at the onset of the wheezing, where our linear model is applicable. It has been observed in tube experiments (Gavriely *et al.* 1989) that the nonlinear (post-onset) frequency response is higher than that at onset. This has been seen theoretically in the nonlinear analysis of the Grotberg & Reiss (1984) model, which was found by Grotberg & Gavriely (1989) to compare favourably with the post-onset behaviour seen in tube experiments (Gavriely *et al.* 1989). As no critical flow speeds are reported for the wheeze experiments, we do not attempt a comparison of onset flow speeds.

A more quantitative comparison is possible with experiments with flexible tubes. Gavriely *et al.* (1987, 1989) have demonstrated that the characteristics of both the collapse phenomenon and the sounds produced in such tubes are similar to those in the lung. Our comparison with their results for flexible tubes should therefore indicate that our model is also applicable to the lung. Gavriely *et al.* (1989) experimentally investigated air-conducting flexible tubes, and found an oscillatory instability following tube collapse. To obtain results using our developing flow model, it is necessary to select an axial position at which to evaluate the developing flow profile. In the experiments a long (60 cm) flexible tube was fastened at either end to a rigid pipe, and air flow through the tube induced by a suction pump at the downstream end. As the driving pressure gradient was increased, collapse and flutter occurred at the downstream end of the tube. The entrance length for a tube is $x_{ENT} = 0.25 a^2 u_{AVG} / \nu$ (where a is the tube radius and u_{AVG} the average fluid velocity) (Schlichting 1955); for the experiment the uncollapsed tube radius $a = 0.325$ cm, $\nu = 0.15$ cm² s⁻¹, and $u_{AVG} = 1600$ cm s⁻¹, so that $x_{ENT} = 280$ cm. Thus, it is clearly appropriate to consider the flow in the collapsed tube section to be developing.

However, the precise appearance of the profile is unclear, as when the flow enters the collapsed section it regains a more pronounced boundary-layer character owing to the constriction. We therefore calculate the stability of the system at several axial locations, and also compare with the results for fully developed flow. These results, along with the experimental data, are shown in table 3, which shows flutter frequencies and critical flow speeds for three different experimental cases. We see that the predicted flutter frequencies are in good agreement with the experimental observations. Similarly, the wavelengths of the instability are close: the theoretically predicted wavelengths are about 3 cm while wavelengths of 3–5 cm were observed experimentally (Gavriely *et al.* 1989). It is not appropriate to compare directly the theoretical and experimental flow speeds, however, as the value measured experimentally is an average over the collapsed tube cross-section. As this cross-section is a dumbbell-like shape, the velocity in the central (channel) section of the collapsed tube (where the oscillations appear) will be lower than that in the outer lobes because of viscous resistance.

b (cm)	f (developing flow, $x_0 = 1$) (Hz)	f (developing flow, $x_0 = 3$) (Hz)	f (Poiseuille flow) (Hz)	f (experimental value) (Hz)
0.081	306	308	307	292
0.070	312	309	308	300
0.037	348	†	362	325

b (cm)	S_{CR}^F (developing flow, $x_0 = 1$) (cm s ⁻¹)	S_{CR}^F (developing flow, $x_0 = 3$) (cm s ⁻¹)	S_{CR}^F (Poiseuille flow) (cm s ⁻¹)	Average S_{CR} experimental (cm s ⁻¹)	Centre S_{CR} (from Fidap) (cm s ⁻¹)
0.081	371	504	619	4880	3950
0.070	344	461	540	2760	1000
0.037	280	†	348	1270	470

† For $b = 0.037$, x_0 must be less than three for validity of the developing flow profile.

TABLE 3. Comparison of theoretical flutter frequencies and critical flow speeds with tube experiments (Gavriely *et al.* 1989).

To estimate the extent to which this flow speed differs from the experimentally measured cross-sectional average, however, requires knowledge of the dimensions of the collapsed tube section, which are not reported by Gavriely *et al.* (1989); dimensions that are given are the half-channel width and cross-sectional area. Flaherty, Keller & Rubinov (1972) numerically obtained shapes for collapsed tubes, to which the experimentally dimensions might be matched, but their model is for a tube with walls of negligible width while in the experiments the width of the tube wall (0.19 cm) was a substantial percentage of the uncollapsed radius (0.325 cm). We therefore consider approximate collapsed tube shapes based on the dimensions that are given and the results of Flaherty *et al.*, and find the flow speeds in these collapsed tube shapes using the finite elements software package FIDAP. As the imprecision in estimating the tube shape and dimensions itself prevents the velocity calculation from being quantitative, only fully developed flow is considered, as this results in an order of magnitude decrease in the required computational resources from those necessary for the calculation of developing flow. The results of these calculations are also shown in table 3, and indicate that for the more collapsed tube shapes (smaller b , when the channel model is most appropriate), the flow speed in the channel section of the tube was likely to have been much closer to our theoretical predictions than the cross-sectional average.

Two observations verify that the flutter instability investigated above (rather than the TSI) is that which is relevant to the tube experiments, and, by extension, the lung. First, the experimentally observed instability is symmetric, while the TSI is antisymmetric, and second, we also calculate the critical flow speed for the TSI to demonstrate that it occurs for much higher flow speeds. For TSI we find a critical average flow speed of approximately 18 500 cm s⁻¹, which is far in excess of both the experimentally measured and theoretically predicted (flutter) values. The frequency of the oscillation for the instability is 11 360 Hz at criticality, which is again several orders of magnitude larger than the experimental or theoretical values. These calculations are for plane-Poiseuille flow; the critical Reynolds numbers for the TSI in developing flows are much higher (Chen & Sparrow 1967).

8. The Tollmien–Schlichting instability

It is clear from the preceding discussion that the TSI is not likely to appear for the thick-walled, air-conveying tubes modelled in the present study, so that we are justified in restricting our attention to flutter. However, in other systems, e.g. when the ratio of wall and fluid densities are similar (so that the mass ratio is closer to unity), the TSI is likely to be significant. While this is not the case in the lung airways, it is for many engineering applications and for physiological applications such as blood flow. In the latter, however, the flows are likely to be fully developed, and in arterial flows significantly pulsatile. The stability of pulsatile flows with compliant boundaries has, however, not been considered to date.

9. Discussion

We have considered the stability of a flexible walled channel conveying a developing flow, showing the existence and behaviour of both a finite wavenumber and long-wave instability. These may appear independently or simultaneously, in the latter case resulting in a codimension two bifurcation point from the base flow. The long-wave instability has not been seen in previous channel studies because it requires the inclusion of transverse variation in the base flow profile. The existence of the long-wave instability may also be of physical interest, as we speculate that it could be related to further tube collapse. We have examined the effect of variation of different system parameters on the instabilities of the system, and have shown, in particular, that the effects found theoretically to destabilize the flutter instability are those that would be expected to characterize the lungs of individuals who are more prone to flow limitation and wheezing, thus providing further support for the theory that pulmonary flow limitation and wheezing are symptomatic of airway collapse and flutter. These qualitative observations are further corroborated by the more quantitative agreement between theoretically predicted and experimentally observed flutter frequencies shown in §7. To compare theoretical and experimental critical flow speeds, however, we have shown that consideration of the geometry of the experimental collapsed tube cross-section is important.

As indicated in the model derivation in §3, the use of the developing flow profile in the stability calculation demands that the axial position at which the profile is evaluated be chosen so that the locally parallel assumption be valid. For the assumption of parallel flow to be completely valid the change of the boundary-layer thickness over a disturbance wavelength must be small by comparison to the channel width. More precisely, it should be the case that $\delta(x_0 + \Delta x) - \delta(x_0) \ll 1$, where $\delta(x_0)$ is the boundary-layer width (non-dimensionalized on half-channel width) a non-dimensional distance x_0 downstream from the mouth of the channel and $\Delta x = 2\pi/k$ is the non-dimensional disturbance wavelength. Similarity analysis of the boundary-layer equations gives $\delta(x_0) \approx 5(\nu^* x_0^* / \hat{u} b^{*2})^{1/2}$ (Schlichting 1955); with this, the condition for slow variation of $\delta(x_0)$ reduces in a straightforward manner to

$$\frac{2\pi}{k R_w S} \ll \frac{1}{25} \left(1 + 10 \left(\frac{x_0}{R_w S} \right)^{1/2} \right). \quad (9.1)$$

The requirement for the developing flow profile itself to be valid, i.e. that the axial position being considered be downstream of the leading edge of the channel wall, is $x \gg (R_w S)^{-1}$ (Batchelor 1967), which is in general less stringent than the above. For the

developing flow profile that we use, the axial position x considered must also satisfy the requirement $x < 0.02R_w S$ (cf. §3.3). We are not guaranteed in advance, however, that on satisfying this condition (9.1) will also be satisfied – this is clearly the case for the long-wave instability. We therefore mention here the possible effect of non-parallelism on the stability calculation. For the TSI non-parallel effects have been shown to be destabilizing for Blasius flow over a single wall (Gaster 1974), and for developing flow in a channel (Garg & Gupta 1981). However, the introduction of non-parallelism also results in great sensitivity to the quantity used to measure instability (e.g. growth in axial or transverse velocity, kinetic energy, etc.), so that it is difficult to quantify the degree to which this is the case, and the magnitude of the effect may be less than was previously thought (Fasel & Konzelmann 1990). For Blasius flow over a single rigid wall a detailed numerical study demonstrated that parallel flow results provide a good leading-order approximation for the desired stability results (Fasel & Konzelmann 1990). A nonlinear analytical study (Hall & Smith 1984) showed that non-parallelism is significant in the development of the instability, determining the eventual state attained by the flow downstream and permitting a smooth bifurcation. The only study of the effect of non-parallelism on flow with a compliant boundary treated the flow over a single compliant wall, and showed that in that geometry non-parallelism slightly destabilizes the TSI and one mode of the flutter instability, and may more significantly destabilize the low-Reynolds number flutter mode (Yeo, Koo & Chong 1994). This destabilizing effect was found to decrease with increasing Reynolds number. It has not been shown whether this result would apply directly to the channel geometry we consider, and the Reynolds numbers in the lung airways we seek to model are high, so that we expect our results should be reasonable in the absence of non-parallel considerations. We have therefore chosen not to undertake an analysis of the non-parallel problem here.

The authors are grateful for the helpful advice of Dr Oliver E. Jensen regarding the early development of this work, and for many useful discussions with Dr Noam Gavriely about our comparisons with experiments. This work was supported by the Department of Defense NDSEG Fellowship program, NSF grant CTS 9013083 and the Whitaker Foundation.

REFERENCES

- BACHELOR, G. K. 1967 *An Introduction to Fluid Dynamics*. Cambridge University Press.
- BENJAMIN, T. B. 1960 Effects of a flexible boundary on hydrodynamic stability. *J. Fluid Mech.* **9**, 513–532.
- BENJAMIN, T. B. 1963 The threefold classification for unstable disturbances in flexible surfaces bounding inviscid flows. *J. Fluid Mech.* **16**, 436–450.
- BENJAMIN, T. B. 1964 Fluid flow with flexible boundaries. In *Proc. of the 11th Intl Congr. Appl. Maths* (ed. H. Görtler), pp. 109–128.
- BERTRAM, C. D. & PEDLEY, T. J. 1982 A mathematical model of unsteady collapsible tube behaviour. *J. Biomech.* **15**, 39–50.
- CARPENTER, P. W. 1984 The effect of a boundary layer on the hydroelastic instability of infinitely long plates. *J. Sound Vib.* **93** (3), 461–464.
- CARPENTER, P. W. & GAJJAR, J. S. B. 1990 A general theory for two- and three-dimensional wall-mode instabilities in boundary layers over isotropic and anisotropic compliant walls. *Theoret. Comput. Fluid Dyn.* **1**, 349–378.
- CARPENTER, P. W. & GARRAD, A. D. 1985 The hydrodynamic stability of flow over Kramer-type compliant surfaces. Part 1. Tollmien–Schlichting instabilities. *J. Fluid Mech.* **155**, 465–510.

- CARPENTER, P. W. & GARRAD, A. D. 1986 The hydrodynamic stability of flow over Kramer-type compliant surfaces. Part 2. Flow induced surface instabilities. *J. Fluid Mech.* **170**, 199–232.
- CHEN, T. S. & SPARROW, E. M. 1967 Stability of the developing laminar flow in a parallel-plate channel. *J. Fluid Mech.* **30**, 209–224.
- COLLINS, M. & SCHOWALTER, W. R. 1962 Laminar flow in the inlet region of a straight channel. *Phys. Fluids* **5**, 1122–1124.
- CONRAD, W. A. 1969 Pressure–flow relationships in collapsible tubes. *IEEE Trans. on Bio-Medical Engng* **16**, 284–295.
- CRAIK, A. D. D. 1991 The continuous spectrum of the Orr–Sommerfeld equation: note on a paper of Grosch & Salwen. *J. Fluid Mech.* **226**, 565–574.
- DAVEY, A. 1973 A simple numerical method for solving Orr–Sommerfeld problems. *Q.J. Mech. Appl. Maths.* **26**, 401–411.
- DRAGON, C. A. & GROTBORG, J. B. 1991 Oscillatory flow and mass transport in a flexible tube. *J. Fluid Mech.* **231**, 135–155.
- DRAZIN, P. G. & REID, W. H. 1981 *Hydrodynamic Stability*. Cambridge University Press.
- FASEL, F. & KONZELMANN, U. 1990 Non-parallel stability of a flat-plate boundary layer using the complete Navier–Stokes equations. *J. Fluid Mech.* **221**, 311–347.
- FLAHERTY, J. E., KELLER, J. B. & RUBINOW, S. I. 1972 Post buckling behavior of elastic tubes and rings with opposite sides in contact. *SIAM J. Appl. Maths* **23**, 446–455.
- GAD-EL-HAK, M. 1986 Boundary layer interactions with compliant coatings: An overview. *Appl. Mech. Rev.* **39**, 511–523.
- GARG, V. K. & GUPTA, S. C. 1981 Nonparallel effects on the stability of developing flow in a channel. *Phys. Fluids* **24**, 1752–1754.
- GARRAD, A. D. & CARPENTER, P. W. 1982 A theoretical investigation of flow-induced instabilities in compliant coatings. *J. Sound Vib.* **85**, 483–500.
- GASTER, M. 1974 On the effects of boundary-layer growth on flow stability. *J. Fluid Mech.* **66**, 465–480.
- GAVRIELY, N., KELLY, K. B. & GROTBORG, J. B. 1987 Forced expiratory wheezes are a manifestation of airway flow limitation. *J. Appl. Physiol.* **62**, 2398–2403.
- GAVRIELY, N., SHEE, T. R., CUGELL, D. W. & GROTBORG, J. B. 1989 Flutter in flow-limited collapsible tubes: a mechanism for generation of wheezes. *J. Appl. Physiol.* **66**, 2251–2261.
- GROSCHE, C. E. & SALWAN, H. 1978 The continuous spectrum of the Orr–Sommerfeld equation. Part 1. the spectrum and the eigenfunctions. *J. Fluid Mech.* **87**, 33–54.
- GROTBORG, J. B. & DAVIS, S. H. 1980 Fluid-dynamic flapping of a collapsible channel: sound generation and flow limitation. *J. Biomech.* **13**, 219–230.
- GROTBORG, J. B. & GAVRIELY, N. 1989 Flutter in collapsible tubes: a theoretical model of wheezes. *J. Appl. Physiol.* **66**, 2262–2273.
- GROTBORG, J. B. & REISS, E. L. 1982 A subsonic flutter anomaly. *J. Sound Vib.* **80**, 444–446.
- GROTBORG, J. B. & REISS, E. L. 1984 Subsonic flapping flutter. *J. Sound Vib.* **92**, 349–361.
- GROTBORG, J. B. & SHEE, T. R. 1985 Compressible-flow channel flutter. *J. Fluid Mech.* **159**, 175–193.
- GUPTA, S. C. & GARG, V. K. 1981 Linear spatial stability of developing flow in a parallel plate channel. *Trans. ASME J. Appl. Mech.* **48**, 192–194.
- HAINS, F. D. & PRICE, J. F. 1962 Effect of a flexible wall on the stability of Poiseuille flow. *Phys. Fluids* **5**, 365.
- HALL, P. & SMITH, F. T. 1984 On the effects of nonparallelism, three-dimensionality, and mode interaction in nonlinear boundary-layer stability. *Stud. Appl. Maths* **70**, 91–120.
- JORDINSON, R. 1970 The flat plate boundary layer. Part 1. Numerical integration of the Orr–Sommerfeld equation. *J. Fluid Mech.* **43**, 801–811.
- KAMM, R. D. & PEDLEY, T. J. 1989 Flow in collapsible tubes: A brief review. *J. Biomech. Engng* **111**, 177–179.
- KATZ, A. I., CHEN, Y. & MORENO, A. H. 1969 Flow through a collapsible tube. Experimental analysis and mathematical model. *Biophys. J.* **9**, 1261–1279.

- LANDAHL, M. T. 1962 On the stability of a laminar incompressible boundary layer over a flexible surface. *J. Fluid Mech.* **13**, 607–632.
- LAROSE, P. G. 1994 Wall–fluid instabilities in compliant channels conveying developing flows. PhD thesis, Department of Engineering Sciences and Applied Mathematics, Northwestern University, Evanston, IL.
- LIN, C. C. 1961 Some mathematical problems in the theory of the stability of parallel flows. *J. Fluid Mech.* **10**, 430–438.
- LUCEY, A. D. & CARPENTER, P. W. 1992 A numerical simulation of the interaction of a compliant wall and inviscid flow. *J. Fluid Mech.* **234**, 121–146.
- LUCEY, A. D. & CARPENTER, P. W. 1993 On the difference between the hydroelastic instability of infinite and very long compliant panels. *J. Sound Vib.* **163**, 176–181.
- MATSUZAKI, Y. & FUNG, Y. C. 1977 Stability analysis of straight and buckled two-dimensional channels conveying an incompressible flow. *Trans. ASME J. Appl. Mech.* **44**, 548–552.
- OLSON, D. E., DART, G. A. & FILLEY, G. F. 1970 Pressure drop and fluid flow regime of air inspired into the human lung. *J. Appl. Physiol.* **28**, 482–494.
- PAÏDOUSSIS, M. P. & ISSID, N. T. 1974 Dynamic stability of pipes conveying fluid. *J. Sound Vib.* **33**, 267–294.
- PAÏDOUSSIS, M. P. & MATEESCU, A. D. 1987 Dynamics of cylindrical shells containing fluid flows with a developing boundary layer. *AIAA J.* **26**, 857–863.
- PIERUCCI, M. & MORALES, P. G. 1990 Effect of finite thickness flexible boundary upon the stability of a Poiseuille flow. *Trans. ASME J. Appl. Mech.* **57**, 1056–1060.
- RILEY, J. J., GAD-EL-HAK, M. & METCALFE, R. W. 1988 Compliant coatings. *Ann. Rev. Fluid Mech.* **20**, 393–420.
- ROTENBERRY, J. M. 1992 Finite-amplitude shear waves in a channel with compliant boundaries. *Phys. Fluids A* **4**, 270–276.
- ROTENBERRY, J. M. & SAFFMAN, P. G. 1990 Effect of compliant boundaries on weakly nonlinear shear waves in channel flow. *SIAM J. Appl. Math.* **50**, 361–394.
- SAPIR, M. H. & REISS, E. L. 1979 Dynamic buckling of a nonlinear Timoshenko beam. *SIAM J. Appl. Maths* **37**, 290–301.
- SCHLICHTING, H. 1934 Laminare Kanaleinlaufströmung. *Z. angew Math. Mech.* **14**, 368–373.
- SCHLICHTING, H. 1955 *Boundary Layer Theory*. McGraw-Hill.
- SHAPIRO, A. H. 1977 Steady flow in collapsible tubes. *J. Biomech. Engng* **99**, 126–147.
- WEAVER, D. S. & PAÏDOUSSIS, M. P. 1977 On collapse and flutter phenomena in thin tubes conveying fluid. *J. Sound Vib.* **50**, 117–132.
- YEO, K. S., KHOO, B. C. & CHONG, W. K. 1994 The linear stability of boundary-layer flow over compliant walls: effects of boundary-layer growth. *J. Fluid Mech.* **280**, 199–225.